Automatic Generation of Chemical Mechanisms for Electrochemical Systems: Solid Electrolyte Interphase Formation in Lithium Batteries

Matthew S. Johnson,[*,†] David Farina Jr.,[‡] Lance Kavalsky,[¶] Judit Zádor,[§] Richard H. West,[‡] Venkatasubramanian Viswanathan,[¶] and William H. Green[*,†]

[†]Department of Chemical Engineering, Massachusetts Institute of Technology, Cambridge, MA 02139, United States

[‡]Department of Chemical Engineering, Northeastern University, Boston, Massachusetts 02115, United States

[¶]Department of Mechanical Engineering, Carnegie Mellon University, Pittsburgh, Pennsylvania 15213, United States

[§]Combustion Research Facility, Sandia National Laboratories, California 94551-0969, United States

E-mail: mjohnson541@gmail.com; whgreen@mit.edu

Abstract

Electrolytes in many lithium ion batteries decompose at the low potentials near the anode. The decomposition products form a layer termed the solid electrolyte interphase (SEI). The composition and growth of the SEI layer significantly affect both the capacity fade and safety of lithium ion batteries. However, SEI formation and growth kinetics are not well understood. In this work, we present an extension of the Reaction Mechanism Generator (RMG) software to automatically generate mechanisms

1

for SEI formation. We extend RMG's solvation correction formulation to account for kinetic solvent effects and demonstrate the accuracy of this technique. We calculate thermochemical parameters for 252 species and rate coefficients for 69 reactions, most with associated solvation corrections. This and additional quantum chemistry data are used to extend RMG's thermodynamic group additivity and solute parameter estimation schemes to handle lithiated species and add 14 new reaction families to RMG. RMG is additionally extended to simulate electrocatalytic systems. Lastly we demonstrate RMG on the decomposition of acetonitrile and ethylene carbonate near a Li(110) anode. While this framework does not yet resolve individual ions, as appropriate thermochemistry estimators are not available, and thus, cannot yet resolve more complex electrochemical pathways, it is able to generate reasonable pathways for SEI formation that agree with important components and intermediates in literature.

Introduction

In many lithium ion batteries, the electrolyte reduces at low potentials near the surface of the anode. While decomposition of the electrolyte is generally undesirable, these decomposition products can form a protective solid electrolyte interphase (SEI) between the anode and electrolyte. This SEI in some cases is selectively permeable protecting the electrolyte from the anode while allowing lithium ions to pass through. The composition and growth of the SEI layer have very significant impacts on the capacity fade and safety of lithium ion batteries. However, the kinetics of SEI formation and growth are not well understood.[1,2]

Much prior work has examined the thermodynamic and/or kinetic barriers to possible liquid and surface reaction pathways.[3–14] However, as far as the authors are aware, the only detailed chemical kinetic mechanism in literature to date is the recent mechanism proposed for formation of an SEI from ethylene carbonate in Spotte-Smith et al. 2022.[15] That mechanism contains 62 species and 900 reactions, with most wells and transition states determined by running optimizations at the ωB97X-V/def2-TZVPPD/SMD level of theory in ethylene

carbonate. All 345 of their associated transition states were identified using the single-ended growing string method.[16] However, the dataset generation and filtering procedure used to generate that mechanism is computationally expensive and electrolyte specific.[6,15] They have also done mechanism work on diglyme as an Mg-ion battery electrolyte, however, as far as we are aware the associated mechanisms were not released in full.[12]

Development and use of kinetic mechanisms is far more developed in gas phase kinetics.[17,18] While many gas phase mechanisms are still developed using tedious manual processes, modern tools for automatic mechanism generation such as the Reaction Mechanism Generator (RMG) software are commonly used.[19–22] RMG generates kinetic mechanisms starting from an initial set of species based on simulations at a set of given reaction conditions. Species are divided into a set of core species that the algorithm has determined are important and a set of edge species that may be important. Upon each iteration, core species are reacted using templates from a database of reaction families to generate new edge species and edge reactions whose associated thermodynamic and kinetic properties are estimated. The time-dependence of core species are then simulated and fluxes through edge reactions to edge species are calculated during the simulation. If the flux to an edge species becomes high enough, the species is added to the core along with any reactions now only involving core species. This iterative procedure continues until the simulations terminate without adding species to the core or causing species to react.[19–22]

RMG has proven to be effective for generating gas phase kinetics mechanisms containing species composed of carbon, hydrogen, and oxygen.[17,23–26] It can also now handle nitrogen, sulfur, and halogen chemistries.[27–30] Additional schemes have been developed within RMG to handle liquid phase systems[31–34] and gas-solid catalytic systems.[35–38] However, no such scheme exists for ionic, electrochemical, or liquid phase catalytic systems. In this work, we extend RMG to lithium-based liquid phase electrocatalytic systems and present test cases related to the radically driven formation of the SEI in lithium ion batteries.

Theory/Development

Species Definition

In any chemical kinetic system it is important to define which configurations of molecules constitute distinct chemical species to be tracked in simulations. This definition also controls which chemical interactions constitute chemical reactions within the system. For every species, RMG needs to reliably estimate thermochemistry,[21] represent resonance structures,[39] and define families for all relevant reactions.[21] Lone ions, with net charges, represent a particular challenge in this respect because currently there are no general high accuracy thermochemistry estimators available for ions. Furthermore, ionic resonance structure generation has not been well studied in this context and solvation correction predictions for lone ions are more challenging than neutral species. Until such capabilities are available, we define all reaction templates such that all reactant and product species are either neutral or Li^+. However, it is worth noting that once RMG is extended to handle arbitrary charged species, that will seamlessly integrate with the work done here.

Gas Phase Quantum Chemistry

We approach liquid phase chemistry by calculating thermochemical and kinetic properties in the gas phase and then correcting them to arbitrary solvents.

We ran most electronic structure calculations at the CCSD(T)-F12/cc-pVDZ-F12//ωB97X-D3/def2-TZVP level, with 1-D hindered rotors at the B3LYP/6-311++G(d,p) level. Molpro was used for the single-point energy calculation, QChem for the optimization and frequency calculations, and Gaussian 16 for the rotor scans. Due to the computational expense, hindered rotor calculations were omitted for a few large species and transition states. Some Transition states (TSs) were identified at the B3LYP/6-311++G(d,p) level rather than ωB97X-D3/def2-TZVP. In these cases we attempted to refine using ωB97X-D3/def2-TZVP, however, if the refining optimization did not converge the associated reactions were computed

at the CCSD(T)-F12/cc-pvdz-F12//B3LYP/6-311++G(d,p) level. Hindered rotor scans are not strictly necessary for accurate calculations at typical SEI temperatures, but they provide additional protection against guessing an incorrect lowest energy geometry.

To facilitate this effort to automatically generate mechanisms for SEI formation, we added a small set of lithium based species to RMG's reference data set and fit a new set of atom energy corrections (AECs) and bond additivity corrections (BACs) for the CCSD(T)-F12/cc-pvdz-F12//ωB97X-D3/def2-TZVP level of theory that included lithium. We were unable to find appropriate reference data that included Li-N or Li-C bonds, so the BACs do not include those bonds. Similarly computed BACs on non-ionic species achieve mean absolute errors (MAE) of ~ 0.7 kcal/mol against experiments.[40]

Transition states were identified manually using bond scans at the B3LYP/6-311++G(d,p) level. The remaining quantum chemistry calculations were done using a version of the Automatic Rate Calculator (ARC) modified to handle lithium species.[41] ARC generates a large number of conformers using RDKit that is dependent on the number of heavy atoms in the molecule.[42] All of these possible conformers are optimized using the MMFF94 forcefield or if the molecule contains lithium the UFF forcefield. The geometries of the ten unique lowest energy conformers where refined at ωB97X-D3/def2-TZVP and the conformer with the lowest energy including zero-point energy (ZPE) at that level of theory was used in subsequent calculations. If a lower energy conformer is found during 1-D hindered rotor scans of wells or transition states, ARC automatically switches to that conformer. Internal reaction coordinate (IRC) calculations were run for every transition state and transition states were confirmed by analysis of the imaginary frequency and either using the IRC or, in cases where the IRC was inconclusive, by manually matching against the bond scans. Arkane[43] was used within ARC to run the statistical mechanical computations, transition state theory, and energy corrections. Submerged barrier reaction calculations assume equilibrium between the

5

bimolecular reactants and the van der Waals well, allowing calculation from

$$k = \frac{k_B T}{h} \frac{Q_{TS}}{Q_R} e^{-\frac{(E_{TS} - E_R)}{RT}} \tag{1}$$

where R and TS denote the reactant and TS states and E denotes the energy, Q denotes the partition function and T the temperature, which should be a good assumption in solvent.[44,45]

Solvation Corrections

RMG's solvation corrections are based on the Abraham and Mintz linear solvation energy relationships

$$\log_{10}(K(298 \text{ K})) = c + eE + sS + aA + bB + lL \tag{2}$$

$$\Delta G_{solv} = -RT \ln(K) \tag{3}$$

$$\frac{\Delta H_{solv}(298 \text{ K})}{1 \text{ kJ/mol}} = c' + e'E + s'S + a'A + b'B + l'L \tag{4}$$

where K is the gas-liquid partition coefficient, ΔG_{solv} is the solvation free energy, R is the gas constant, T is the temperature, ΔH_{solv} is the enthalpy of solvation, $c, e, s, a, b, l, c', e', s', a', b', l'$ are solvent specific parameters and E, S, A, B, L are solute specific parameters.[31–34,46–49] This approach allows RMG to be applied to any arbitrary solvent, provided that the solvent-specific parameters are known. In order to fit these parameters, we need to compute ΔG_{solv} and ΔH_{solv}. While SMD[50–52] is popular, in our hands the recent versions of COSMO-RS[53–55] are even more accurate, at least for non-ionic species.[34] For our purposes, we compute solvation free energies based on the optimized gas phase geometries, running energy and COSMO-RS calculations at the COSMO-RS/BP86/TZVPD-FINE level.

To fit solvent parameters we took the intersection of the set of experimental solute parameters from Chung et al. 2022[34] and COSMO-RS's internal database. For each of those solutes we computed ΔG_{solv} and ΔH_{solv} in the solvent of choice and then linearly regressed the solvent parameters through Equations 2 and 4. To fit solute parameters for

both species and transition states, we took experimental solvent parameters for 24 more accurate polar solvents from the RMG-database. We then computed the ΔG_{solv} for the solute in each selected solvent and linearly regressed the solute parameters against Equation 2. Mean absolute fitting errors for the solute parameters for non-lithiated species were typically < 0.25 kcal/mol, singly lithiated species were ~ 0.5 kcal/mol, doubly lithiated species were typically $2 - 3$ kcal/mol and Li^+ was 1.78 kcal/mol.

The transition state solvation corrections were implemented for a given rate coefficient

$$k_{gas}(T) = A \left(\frac{T}{1 \text{ K}} \right)^n e^{-\frac{E_a}{RT}} \tag{5}$$

by first computing

$$\Delta S_{solvTS}(298 \text{ K}) = \frac{\Delta H_{solvTS}(298 \text{ K}) - \Delta G_{solvTS}(298 \text{ K})}{298 \text{ K}} \tag{6}$$

then computing

$$\Delta\Delta H_{solv} = \Delta H_{solvTS}(298 \text{ K}) - \Delta H_{solvReactants}(298 \text{ K}) \tag{7}$$

$$\Delta\Delta S_{solv} = \Delta S_{solvTS}(298 \text{ K}) - \Delta S_{solvReactants}(298 \text{ K}) \tag{8}$$

and then correcting using

$$k_{solv}(T) = k_{gas}(T)e^{\frac{\Delta\Delta S_{solv}}{R} - \frac{\Delta\Delta H_{solv}}{RT}} = A \left(\frac{T}{1 \text{ K}} \right)^n e^{\frac{\Delta\Delta S_{solv}}{R} - \frac{\Delta\Delta H_{solv} + E_a}{RT}} \tag{9}$$

where A, n and E_a are modified Arrhenius parameters, TS denotes properties of the transition state and Reactants denotes properties of the reactants, $\Delta\Delta$ denotes the difference in the solvation correction for the associated property between the transition state and reactants, k_{gas} denotes that gas phase rate coefficient and k_{solv} denotes the rate coefficient in solvent.

7

Thermochemistry Estimation

In total, the thermochemical and solute parameters of 247 species were added to RMG's thermochemistry and solute libraries. We additionally linearly regressed 12 new lithium groups for both RMG's thermochemistry group additivity scheme and for RMG's group additivity scheme for solute parameters from the calculated data. The groups include lithium bonded to S, O, N and C. These enable RMG to estimate the thermochemistry of arbitrary solvated lithiated species.

The linear free energy relationships used by RMG to correct the Pt(111) adsorption thermochemical contributions to other metallic surfaces do not extend to non-d-block metals and could not be used for lithium. We first generated a small thermochemistry dataset for surface species. We used Pynta[56] to automate the associated quantum chemical calculations and to compute the enthalpy and entropy of reactions at 298 K on Li(110) in the harmonic limit, for a set of reactions designed to include only 7 target adsorbates and gas phase species. All periodic surface DFT calculations in this work were run on a 3×3×4 slab, freezing the bottom two layers, with a (3×3×1) k-point grid using the BEEF-vdW[57] functional with PBE-KJPAW pseudo-potentials and a kinetic energy cutoff of 50 Ry as implemented in Quantum Espresso. Decomposing the overall enthalpies and entropies of reaction evaluated with periodic DFT gives a simple linear system of equations for the individual enthalpies and entropies of formation at 298 K. Substituting in values for the gas phase species properties from high accuracy calculations in this work or literature[30,58–60] gives a trivial system of equations for the enthalpies and entropies of formation at 298 K for the target adsorbates. This approach is similar to that used in Blondal et al.[36] Heat capacity information for these species was taken from the values in the RMG-database for the same adsorbate on Pt(111). We then used the thermochemistry of those adsorbates and data from the Pt(111) adsorption groups to develop a new set of 10 lithium metal adsorption groups, including groups with surface bonds to C, N, O, F, and H. This allows RMG to estimate the thermochemistry of all such species adsorbed on Li(110).
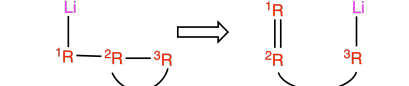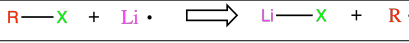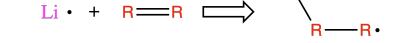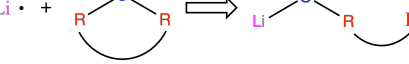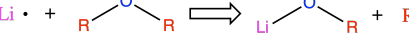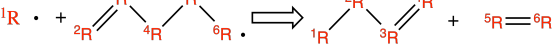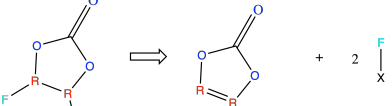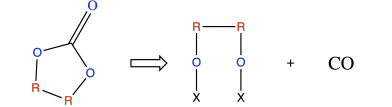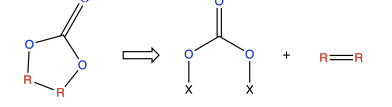
Prediction of the solvation free energy of adsorbed species is not well studied. At present, we treat the solvation and adsorption corrections largely independently. For an adsorbed species we replace the bonds to surface atoms with bonds to hydrogen atoms and calculate the solute parameters. This approximates the solute parameters of adsorbed species as those of the desorbed hydrogenated species. We do not correct for solvent interactions with empty sites on the metal surface.
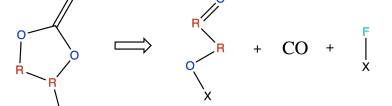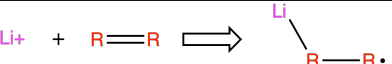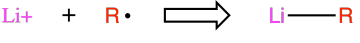
Kinetics

69 calculated reactions were added to RMG's reaction libraries and 14 new reaction families shown in Table 1 were developed and trained.[61] Of these new families, the 7 non-surface and non-electrochemical families were developed to handle common direct reactions with lithium and reactions unique to lithiated species. Except for `R_Addition_MultipleBond_Disprop` they were trained on reactions calculated using ARC.[28] For `R_Addition_MultipleBond_Disprop`, which was confirmed in scans to be barrierless, we scanned the path of the reaction and then calculated frequencies and energies at each point allowing us to compute the rate coefficients using canonical variational transition state theory (CVTST) at the same level of theory. The surface reactions associated with new families were developed based on literature. The carbonate reaction families[9,62] assume sticking coefficients of 0.2. `Surface_Lithium_Addition` uses the parameters for the analogous H^+ ion reaction in Hansen et al. 2014.[63] Additionally 5 surface reactions (not associated with new families) were computed at the same level of theory as the adsorbed species thermochemistry calculated earlier, using Pynta and Harmonically Forced Saddle Point searching (HFSP) to automate the rate coefficient computation.[56]

The 12 liquid phase electrochemical reactions are concerted reactions with an association step and an electrochemical step. The rate coefficients for the electrochemical steps were first computed with Marcus theory using the four-point method with a geometric mean as advocated for in López-Estrada et al.[64] We first compute Gibbs free energies G_{cgn}, G_{ngn}, G_{cgc} and G_{ngc}, where agb denotes calculating using the geometry of a and the charge of b

9

Table 1: Added reaction families. Within the templates, red R denotes any atom, black X denotes a surface site and green X denotes a halogen. The graphics are intended to illustrate the reaction type and are not always as general as the actual template; they also omit vacant surface sites and electrons. All electrochemical families draw their electrons from the metal surface at a distance specified in the simulation parameters.

Family	Reactions	Template
1,2_Elimination_LiR	13	$^1R{-}^2R$ with Li and ^3R ⟹ $^1R{=}^2R$ + Li${-}^3R$
1,2_Intra_Elimination_LiR	5	$^1R{-}^2R{-}^3R$ with Li ⟹ $^1R{=}^2R$ ... ^3R with Li
Li_Abstraction	4	$R{-}X$ + Li· ⟹ Li${-}X$ + R·
Li_Addition_MultipleBond	5	Li· + $R{=}R$ ⟹ Li${-}R{-}R$·
Li_NO_Ring_Opening	6	Li· + (O ring with R, R) ⟹ Li(O)R R·
Li_NO_Substitution	20	Li· + R(O)R ⟹ Li(O)R + R·
R_Addition_MultipleBond_Disprop	2	^1R· + $^2R{-}^3R{=}^4R{-}^5R{=}^6R$ ⟹ $^1R{-}^2R{-}^3R{=}^4R$ + $^5R{=}^6R$
Surface_Carbonate_2F_Decomposition	1	(carbonate ring, F, F, X) ⟹ (carbonate ring) + 2 F–X
Surface_Carbonate_CO_Decomposition	1	(carbonate ring) ⟹ (R–R, O, O, X, X) + CO
Surface_Carbonate_Decomposition	1	(carbonate ring) ⟹ (O(C=O)O, X, X) + R=R
Surface_Carbonate_F_CO_Decomposition	1	(carbonate ring, F) ⟹ (product) + CO + F–X
Surface_Lithium_Addition*	1	Li⁺ + (R=X) ⟹ R(Li)–X
Cation_Addition_Multiple_Bond*	7	Li+ + $R{=}R$ ⟹ (Li)R${-}R$·
Cation_R_Recombination*	5	Li+ + R· ⟹ Li${-}R$

*Electrochemical families

and c denotes the charged geometry/state and n denotes the neutral geometry/state, in gas phase with no hindered rotors. We are then able to estimate λ_i needed for Marcus theory using the recommended geometric mean[64]

$$\lambda_i(T) = \sqrt{(G_{cgn}(T) - G_{ngn}(T))(G_{ngc}(T) - G_{cgc}(T))} \tag{10}$$

where λ_i is the internal reorganization energy. We fit the temperature dependence of λ_i to a third order polynomial

$$\lambda_i(T) = a_1 + a_2 T + a_3 T^2 + a_4 T^3 \tag{11}$$

and are then able to compute λ_o assuming that the distance from the electron source is large compared to the radius of the molecule

$$\lambda_o = N_a \frac{e(N_{ep} - N_{er})^2}{8\pi\epsilon_0 r}\left(\frac{1}{n^2} - \frac{1}{\epsilon}\right) \tag{12}$$

where λ_o is the outer reorganization energy, e is the fundamental charge, N_a is Avogadro's number, N_{ep} is the number of electrons in the products, N_{er} is the number of electrons in the reactants, ϵ_0 is the vacuum permittivity, r is the molecular radius (computed from McGowan volumes), n is the solvent index of refraction and ϵ is the relative permittivity of the solvent. We can then use Marcus theory to compute the Gibbs free energy of the transition state using

$$\Delta G^{\ddagger} = \frac{(\Delta G^0 + \lambda_o + \lambda_i)^2}{4(\lambda_o + \lambda_i)} \tag{13}$$

where ΔG^0 is the Gibbs free energy of reaction (computed from G_{cgc} and G_{ngn}) and $\Delta G^{\ddagger}$ is the Gibbs free energy of the transition state. We then are able to compute the rate coefficient using transition state theory

$$k(T) = \kappa(d)\frac{k_B T}{h}e^{-\frac{\Delta G^{\ddagger}}{RT}} \tag{14}$$

where d is the distance from the electrode. We adopt the approach from Spotte-Smith et al.

11

assuming that $\kappa(d) = e^{-1.2x10^{10}d}$ where d is in meters.[6] This gives the rate coefficient for the electrochemical step. For a sequence

$$Li^+ + A + e^- \leftrightarrow^1 Li^+ - A + e^- \leftrightarrow^2 LiA \tag{15}$$
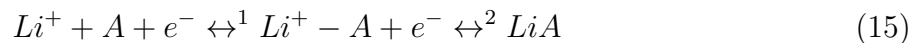
we compute the overall rate coefficient assuming the first step rapidly equilibrates and has a much smaller barrier than the electrochemical step giving us

$$k_{12} = K_1 k_2 \tag{16}$$

.where K_1 is the equilibrium constant for step (1), k_2 is the Marcus theory rate coefficient for the electrochemical step and k_{12} is the overall rate coefficient.

In addition to the above reactions, we include in the associated reaction library the electrochemical reaction

$$\text{Li}^+ + \text{e}^- \longrightarrow \text{Li} \tag{17}$$

assuming a fast 1 ns timescale at 0 V and a symmetry factor of $\beta = 0.5$ based on the lower bound on solvent reorganization time for water used in Hansen et al. 2014.[63] It should be noted our results are not sensitive to this value as most lithiated species are formed through electrochemical reactions with Li^+ rather than reaction with Li.

Kinetic Solvent Effects

We implemented a system within RMG to account for the kinetic solvent effect in the new families. Here, we define the transition state Abraham solute parameters as a sum of contributions from the reactant, product and reaction center

$$P_{TS} = (1 - x)P_R + xP_P + \Delta P_{rxncenter} \tag{18}$$

12

where P is an arbitrary Abraham parameter, P_{TS} denotes the parameter of the transition state, P_R denotes the reactant parameter, P_P denotes the product parameter, x is a measure of how different the transition state is from the reactants, and $\Delta P_{rxncenter}$ is a correction associated with the solvation of the reaction center of the transition state. We are assuming here based on the Hammond-Leffer postulate[65] that the closer the transition state is to the reactant or products the more the solute properties will be similar. We measure x based on the uncorrected activation barrier as

$$x = \frac{|E_a|}{|E_a| + |G_P - E_a - G_R|} \tag{19}$$

where E_a is the uncorrected activation barrier, G_P is the Gibbs free energy of the solvated product and G_R is the Gibbs free energy of the solvated reactant. With these in place we can calculate $\Delta P_{rxncenter}$ for any reaction we have solvation data for. Within RMG's automatic tree generation (ATG) framework[61] at each node in the tree we average $\Delta P_{rxncenter}$ for every parameter. When a new reaction is estimated we take these parameters from where the gas phase kinetics were estimated in the tree and compute the transition state parameters using Equations 18 and 19. As described before in Equations 5-9 the transition state parameters can be used to correct for the kinetic solvent effect. Figure 1 shows a histogram of errors with and without this solvation correction in a 50:50 ethylene carbonate and dimethyl carbonate solvent at 298 K for the Li_NO_Substitution family (19 reactions). The mean absolute errors in $\ln(k)$ for the uncorrected and corrected cases are 10.24 and 5.03 respectively. In this case the corrections represent a two order of magnitude improvement in accuracy at 298 K.

Forbidden Structures

When running RMG it is important to ensure that we do not generate species and reactions that are unphysical, or unimportant species that we are unable to estimate important
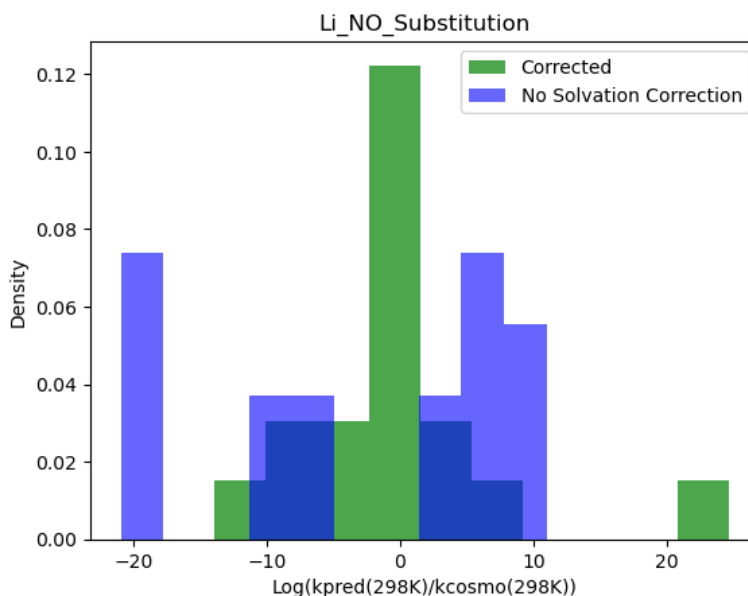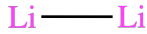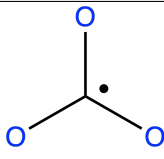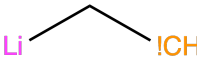
Figure 1: Histogram of leave-one-out errors against the solvent corrected training reactions for `Li_NO_Substitution` for no solvent correction and solvent correction using estimated transition state solute parameters. The mean absolute errors in $\ln(k)$ for the uncorrected and corrected cases are 10.24 and 5.03 respectively.

properties for. The new forbidden structures added to RMG are listed in Table 2. Since the surface species framework treats Lithium atoms distinctly from surface sites allowing Lithium to plate within the model is not feasible as it will result in sites being improperly blocked. In particular, since in this work we simulate at fixed Li^+ concentration, plating of Li^+ would be a null reaction as it should not affect any concentrations in the simulation. Lithium dimerization is also forbidden. We have also forbidden physically adsorbed species in general as such structures are often not stable on lithium.[9,62] Additionally, we found in scans at the B3LYP/6-311++G(d,p) level that the carbonate groups with the radical on the center carbon do not participate in bimolecular radical reactions the same way radicals usually do. We had significant difficulties in identifying transition states for these reactions; however, based on scans we believe that they at least have significantly higher barriers than is typical for similar reactions. For this reason we have forbidden these reactions. We have also forbidden species with lithium ionically bonded to a carbon that is also bonded to a more electronegative atom. While these structures can be optimized, the resulting structure

14

Table 2: Added non-trivial forbidden structures. Within the templates, Orange !CH denotes any atom that is not a carbon or hydrogen atom and black X denotes a surface site.

Name	Forbidden	Reason Forbidden	Template
LiX	Globally	Lithium plating on the surface should not remove reactive sites	
Li-Li	Globally	Disallow lithium dimer formation	
VDW	When $X = Li$	Most species tend to only chemisorb to Li metal surfaces.	
CO3	Bimolecular reactions involving the radical site	These radical sites were found to be much harder to interact with in scans than is typical.	
LiCONSFCl	Globally	These structures tend to either not optimize or most of the negative charge resides on the !CH atom.	

commonly results in the lithium atom being much closer to the electronegative atom and most of the negative charge not being on the carbon so the optimized structure does not seem to be the target species. For now, as these structures are high in energy we choose to forbid them.

Simulations

Before this work, RMG was mostly limited to constant temperature and pressure gas-phase batch reactors, constant temperature and volume liquid-phase batch reactors, and constant temperature and volume gas-phase catalytic systems. RMG also did not support electrochemical reactions. To enable simulation of electrochemical reactions and liquid phase cat-

alytic systems we first upgraded the ReactionMechanismSimulator.jl (RMS),[66,67] a Julia software for general reaction mechanism simulation, to handle electrochemical reactions using the framework of Hansen et al. 2014[63] and to simulate liquid phase catalytic systems. We then developed a framework that enabled us to easily integrate any RMS reactor configurations into RMG allowing us to run RMG on liquid phase electrocatalytic systems such as the SEI.

The SEI involves highly complex phase behavior and transport that are difficult to resolve in a kinetic model. In this work we considered two very simple scenarios. In the first scenario we targeted initial SEI formation simulating the liquid near the anode as a constant temperature, volume, and potential liquid phase at 298 K, 0 V relative to the anode and with a 0 nm distance from the anode (for Marcus theory evaluations) and the anode as a constant temperature, area, and potential surface phase with a 1×10^5 m^{-1} surface area to liquid volume ratio. In the second scenario we targeted SEI growth simulating a constant temperature, volume, and potential liquid phase alone at 298 K, 0.3 V potential relative to the anode, and a 1 nm distance from the anode. While in the first scenario we used viscosity parameters associated with the electrolyte, for the SEI growth scenario we fixed the viscosity at 5×10^7 Pa·s, resembling that of a polymer, to better represent transport limitations within the SEI. In all liquid phases we simulated with the electrolyte fixed at its pure component concentration and Li^+ fixed at 15 mol/m^3, a typical concentration in a battery, and with the solvent concentration fixed. These constant concentration conditions ensure our electrolyte and Li^+ do not deplete. Initially systems have bare surfaces and start with only the liquid solvent and dissolved Li^+ at nonzero concentrations.

For species selection within RMG we utilized the branching algorithm[22] and simulated the SEI formation scenario only out to short timescales dependent on the electrolyte while all SEI growth scenarios were simulated out to 1000 s. For this demonstration we limited the number of C, N, and O atoms as appropriate to prevent extensive polymerization.

16

Results

Acetonitrile Decomposition on Lithium

We first considered acetonitrile (ACN) a commonly studied electrolyte.[68–70] Experiment-based solvent and viscosity parameters for ACN were drawn from the RMG-database. For the SEI formation scenario study we simulated out to 1000 s and RMG converged at 94 species.

A flux diagram of the mechanism simulated at the SEI formation conditions at 1 second is presented in Figure 2. In this model ACN primarily reacts with Li^+ to form the radical with SMILES [Li]N=[C]C which mostly terminates via radical recombination to form [Li]N=C(C)C(C)=N[Li], but can also react further with Li^+ and ACN to polymerize. The surface is predicted to be mostly covered by dissociative adsorption products of ACN and adsorbed [Li]N=[C]C. In general, however the mechanism predicts ACN will not appreciably decompose at these conditions. The lack of liquid phase decomposition is in good agreement with literature.[68–70] However, ACN is expected to decompose on the metal surface.[68] The lack of surface decomposition in the model is likely because currently the adsorbates must desorb into ACN as neutral species and because we have only implemented one electrochemical reaction family on the surface.

Ethylene Carbonate Decomposition on Lithium

For our second electrolyte we examined ethylene carbonate (EC), perhaps the most common lithium ion battery electrolyte component, which unlike ACN is known to decompose in the liquid phase. Solvent parameters for ethylene carbonate were computed using the methods described in the Solvation Corrections section and viscosity parameters were drawn from those available in the RMG-database for diethyl carbonate. For EC we ran the SEI formation simulation out to only 1 μs due to high reactivity at those conditions. We ran RMG until there were 75 core species, when the fluxes in the mechanism were converged for our
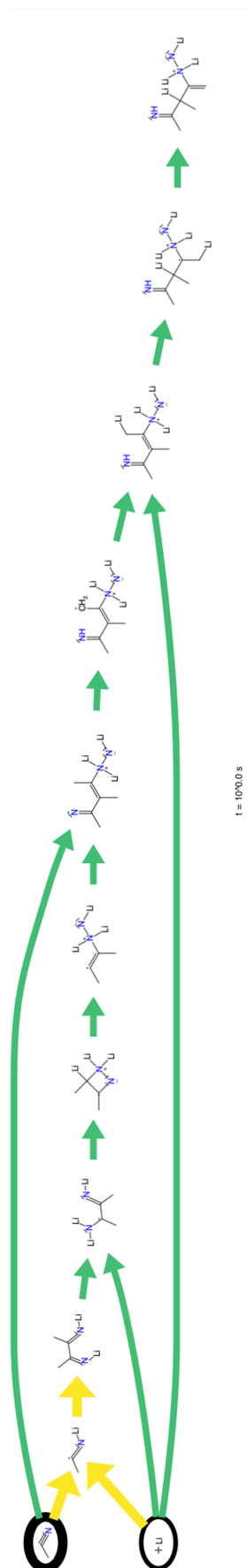
17

Figure 2: Flux diagram for the generated acetonitrile mechanism for the SEI formation condition at 1 second. Larger yellower arrows denote larger fluxes while smaller purpler arrows denote smaller fluxes. Larger circles around species denote higher concentration species while smaller circles denote lower concentration species.

18

Figure 3: Flux diagram for the SEI growth scenario for ethylene carbonate at 10 seconds. Larger yellower arrows denote larger fluxes while smaller purpler arrows denote smaller fluxes. Larger circles around species denote higher concentration species while smaller circles and no circles denote lower concentration species.
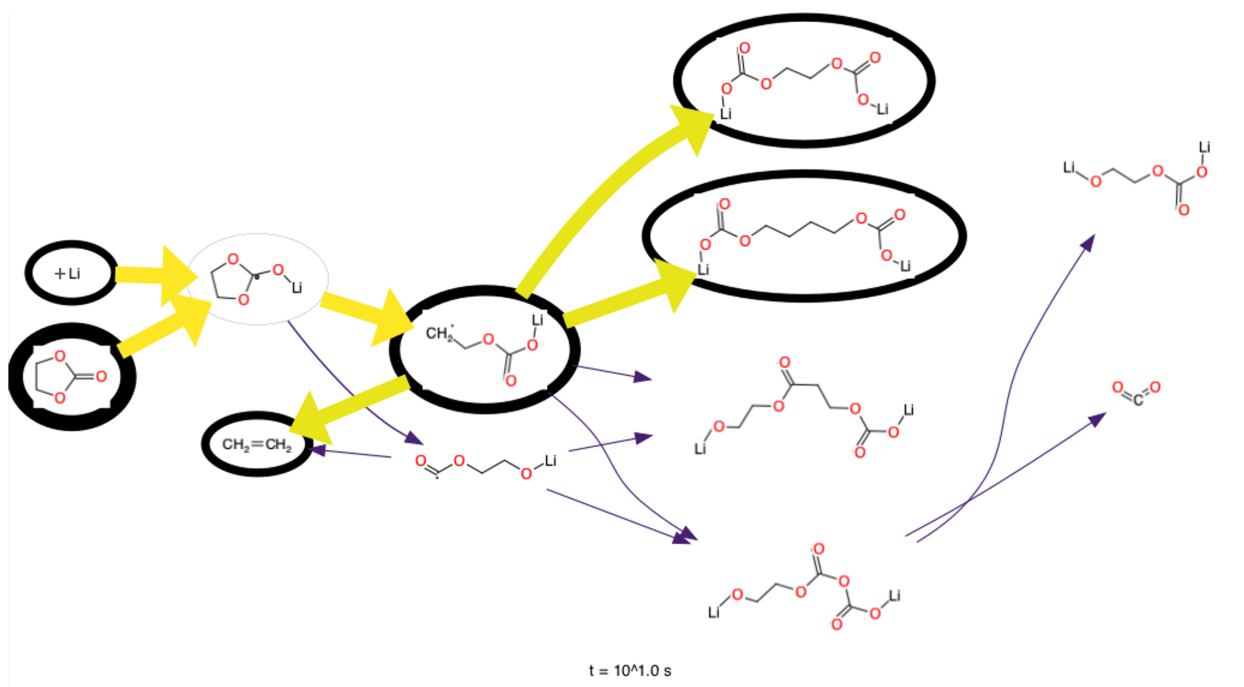
19

scenarios. Interestingly, despite the significant differences in viscosity the two scenarios result in largely the same pathways. Viscosity changes affect diffusion limitations for bimolecular reactions and can strongly affect competition between bimolecular and unimolecular reactions. However, in this case it seems that the high flux pathways do not involve significant competition between bimolecular and unimolecular pathways. Additionally, in the SEI formation scenario we do not predict much chemistry happening on the surface relative to the liquid phase, with the surface being primarily covered with CO_3.

A flux diagram showing the highest fluxes in this mechanism simulated at the SEI growth scenario study conditions at 10 s is available in Figure 3. The pathways in this flux diagram are similar to those in the SEI formation scenario, although the time scales at which chemistry occurs are drastically different between the two cases. The SEI growth scenario predicts a volumetric current draw for the SEI growth chemistry of 3×10^6 A/m^3.

Within Figure 3 we see major intermediates: [Li]O[C]1OCCO1 and [Li]OC(=O)OC[CH2], and major products: [Li]OC(=O)OCCOC(=O)O[Li] (LEDC), [Li]OC(=O)OCCCCOC(=O)O[Li] (LBDC) and C_2H_4. All of these intermediates and products are expected based available experimental data, literature and the Spotte-Smith mechanism[1,15,71] except for LBDC. Apart from the reaction that produces LBDC all of the high flux (yellow arrow) pathways are in the Spotte-Smith mechanism.

RMG produces LBDC from the reaction

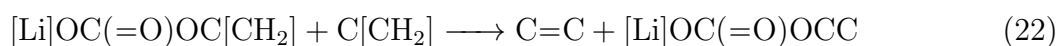$$2\,[Li]OC(=O)OC[CH_2] \longrightarrow [Li]OC(=O)OCCCCOC(=O)O[Li] \tag{20}$$
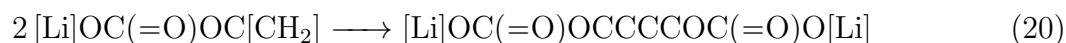
which is a very fast radical recombination generated by RMG and verified to be barrierless by scanning along the reaction bond with DFT. This reaction competes directly with

$$2\,[Li]OC(=O)OC[CH_2] \longrightarrow [Li]OC(=O)OCCOC(=O)O[Li] + C_2H_4 \tag{21}$$
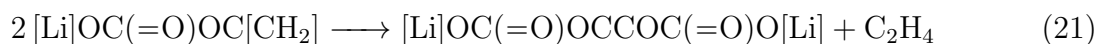
a R_Addition_MultipleBond_Disprop reaction which is included in both mechanisms and

20

noted as an important path in Spotte-Smith et al. 2022. Their approach likely misses the paths to LBDC because the mechanism was developed based on searching for paths between sets of starting materials and experimentally expected products using Kinetic Monte Carlo, and LBDC is not an expected product.[15] We are not aware of any studies of the R_Addition_MultipleBond_Disprop reactions. Upon further examination we discovered these reactions were barrierless so we calculated two cases with CVTST at CCSD(T)-F12/cc-pvdz-F12//ωB97X-D3/def2-TZVP level as mentioned earlier. One of these reactions was

$$[\text{Li}]\text{OC}(=\text{O})\text{OC}[\text{CH}_2] + \text{C}[\text{CH}_2] \longrightarrow \text{C}=\text{C} + [\text{Li}]\text{OC}(=\text{O})\text{OCC} \tag{22}$$

which we considered a good surrogate for the reaction in Equation 21. Using the associated rate coefficient for that reaction implies that the two competing reactions have fast rate coefficients that are within a factor of 2 of each other at 298 K and become nearly indistinguishable when diffusion limitations are accounted for. Recombination reactions are well studied and very fast making it difficult to argue currently that the R_Addition_MultipleBond_Disprop reaction should be appreciably faster than the recombination reaction. While LBDC has not been observed experimentally, that does not preclude it from being an intermediate in this process.

More generally, RMG is able to produce some radical pathways that are similar to the more complex electrochemical steps in the Spotte-Smith mechanism, such as those that lead to Li_2CO_3 and [Li]OCCOC(=O)O[Li] (DLEMC). However, without including charged species it is not easy to represent these faster electrochemical pathways.

Discussion

Overall, we have built a solid framework that enables automatic generation of lithium-based electrocatalytic mechanisms in RMG. As far as the authors are aware this is the first automatic mechanism generation framework for electrocatalytic systems. It is worth

21

contrasting our framework conceptually with that used in Spotte-Smith et al. 2022 and Spotte-Smith et al. 2023.[12,15]

The Spotte-Smith approach starts by manual construction of a large database of thermochemistry in the desired solvent of all species that might be important in connecting overall reactants to expected overall products. Then all possible reactions within a 2D graph representation are generated between all species in the dataset and filtered based on a range of different criteria. Kinetic Monte Carlo (KMC) simulations are then run with constant forward rate coefficients and important reaction sequences are traced backwards from the selected desired products and compiled together to a set of reactions/species considered important. Then a manually selected subset of the associated transition states are searched for using AutoTS and single-ended growing string methods enabling computation of the associated rate coefficients.

In contrast, RMG only takes in the initial species and reaction conditions. Reactions are generated as needed using specific templates for known important reaction classes from the RMG-database. Thermochemistry and kinetics are estimated using using RMG-database libraries and estimators. RMG iteratively runs simulations of identified important species/reactions broadly following the flux to identify additional important species and reactions until convergence where it outputs a chemical mechanism. In practice, these mechanisms are often refined to accuracy iteratively using sensitivity and flux analyses to identify important reactions and quantum chemistry calculations to integrate with the RMG-database to improve libraries and estimators and add new reaction families.[17]

Our approach, at least in principle, is significantly easier, more automated, faster, and much more computationally efficient. Additionally, RMG does not require any assumptions about the final products and is in a broad sense able to apply knowledge learned within its databases from one application to improve performance on other applications. However, RMG is heavily reliant on the accuracy of its estimators and comprehensiveness of its templates. The Spotte-Smith approach instead uses quantum chemistry calculations for all

22

involved species and identified reactions. While very computationally expensive this allows them to mostly circumvent a number of important limitations in our approach. While we have developed machine learning approaches and workflows that are able to automate much of the data integration[20,61,72] and we have made a very significant push that looks quite promising in this work, many additional calculations are still needed. The most glaring area of need is the ability to estimate the thermochemistry of lone ions in solution. Many very important more complex electrochemical reaction sequences cannot be accurately approximated as neutral concerted reactions as done in this work. The next most glaring area of need is development of a much more comprehensive enumeration of important templates for electrochemical systems and training data for the associated kinetics estimators.

Based on literature and calculated errors, the workflow presented for computing parameters accumulates mean absolute errors (MAE) of approximately ~ 0.8 kcal/mol in the energy calculations, ~ 0.5 kcal/mol from the COSMO-RS solvation correction,[34] and ~ 0.5 kcal/mol from solute parameter fitting for singly lithiated species. This gives us results that are solvent agnostic with a total MAE of only ~ 1.8 kcal/mol in theory. However, in order to get to that number we have to assume that the COSMO-RS errors in the solvation free energy of lithiated species are similar to those of the organic species examined in Chung et al. 2022. We are also ignoring multi-lithiated species that have significantly higher fitting errors that might put the number closer to ~ 4 kcal/mol. Additionally, fitting errors on the only lone ion calculated, Li^+, while less than some multi-lithiated species were 1.78 kcal/mol. It is clear that fitting errors are significant contributors to error in this workflow, suggesting that we may be able to improve our accuracy on lithiated species and ions significantly by fitting a more complex solvation correction model.

These electrocatalytic systems have many important reactions between highly reactive species that have diffusion limitations. It may be beneficial to move beyond RMG's current diffusion limitation models to one that properly accounts for how species reactivity interacts with diffusion limitations.[73]

Conclusions

We have presented and demonstrated an extension of the Reaction Mechanism Generator software for automatic generation of chemical kinetic mechanisms in lithium based electro-catalytic systems. Furthermore, we have presented a framework for calculating the thermo-chemistry and kinetics of the involved species and reactions accounting for species solvation free energy and kinetic solvent effects. We demonstrate these contributions by modeling the decomposition of acetonitrile and ethylene carbonate electrolytes near a lithium anode during SEI formation and growth. We hope to extend this framework in the future to handle general charged species and more complex electrochemical reactions.

Acknowledgements

References

(1) Horstmann, B.; Single, F.; Latz, A. Review on multi-scale models of solid-electrolyte interphase formation. 2019.

(2) Annevelink, E. et al. AutoMat: Automated materials discovery for electrochemical systems. *MRS Bulletin* **2022**, *47*, 1036–1044.

(3) Kumar, H.; Detsi, E.; Abraham, D. P.; Shenoy, V. B. Fundamental Mechanisms of Solvent Decomposition Involved in Solid-Electrolyte Interphase Formation in Sodium Ion Batteries. *Chemistry of Materials* **2016**, *28*, 8930–8941.

(4) Blau, S. M.; Patel, H. D.; Spotte-Smith, E. W. C.; Xie, X.; Dwaraknath, S.; Persson, K. A. A chemically consistent graph architecture for massive reaction networks applied to solid-electrolyte interphase formation. *Chemical Science* **2021**, *12*, 4931–4939.

(5) Purushotham, U.; Takenaka, N.; Nagaoka, M. Additive effect of fluoroethylene and difluoroethylene carbonates for the solid electrolyte interphase film formation in sodium-ion batteries: A quantum chemical study. *RSC Advances* **2016**, *6*, 65232–65242.

(6) Spotte-Smith, E. W. C.; Blau, S. M.; Xie, X.; Patel, H. D.; Wen, M.; Wood, B.; Dwaraknath, S.; Persson, K. A. Quantum chemical calculations of lithium-ion battery electrolyte and interphase species. *Scientific Data* **2021**, *8*, 1–15.

(7) Wang, Y.; Balbuena, P. B. Theoretical insights into the reductive decompositions of propylene carbonate and vinylene carbonate: Density functional theory studies. *Journal of Physical Chemistry B* **2002**, *106*, 4486–4495.

(8) Xie, X.; Clark Spotte-Smith, E. W.; Wen, M.; Patel, H. D.; Blau, S. M.; Persson, K. A. Data-Driven Prediction of Formation Mechanisms of Lithium Ethylene Monocarbonate

with an Automated Reaction Network. *Journal of the American Chemical Society* **2021**, *143*, 13245–13258.

(9) Zhang, Y.; Krishnamurthy, D.; Viswanathan, V. Engineering Solid Electrolyte Interphase Composition by Assessing Decomposition Pathways of Fluorinated Organic Solvents in Lithium Metal Batteries. *Journal of The Electrochemical Society* **2020**, *167*, 070554.

(10) Zhang, Y.; Viswanathan, V. Design Rules for Selecting Fluorinated Linear Organic Solvents for Li Metal Batteries. *Journal of Physical Chemistry Letters* **2021**, *12*, 5821–5828.

(11) Barter, D.; Spotte-Smith, E. W. C.; Redkar, N. S.; Khanwale, A.; Dwaraknath, S.; Persson, K. A.; Blau, S. M. Predictive stochastic analysis of massive filter-based electrochemical reaction networks. *Digital Discovery* **2023**, *2*, 123–137.

(12) Spotte-Smith, E. W. C.; Blau, S. M.; Barter, D.; Leon, N. J.; Hahn, N. T.; Redkar, N. S.; Zavadil, K. R.; Liao, C.; Persson, K. A. Chemical Reaction Networks Explain Gas Evolution Mechanisms in Mg-Ion Batteries. *Journal of the American Chemical Society* **2023**, *145*, 12181–12192.

(13) Kavalsky, L.; Hegde, V. I.; Viswanathan, V. AutoCat. `https://github.com/aced-differentiate/auto_cat`, 2022.

(14) Kavalsky, L.; Hegde, V. I.; Muckley, E.; Johnson, M. S.; Meredig, B.; Viswanathan, V. By how much can closed-loop frameworks accelerate computational materials discovery? **2022**,

(15) Spotte-Smith, E. W. C.; Kam, R. L.; Barter, D.; Xie, X.; Hou, T.; Dwaraknath, S.; Blau, S. M.; Persson, K. A. Towards a Mechanistic Model of Solid-Electrolyte Interphase Formation and Evolution in Lithium-ion Batteries. **2022**,

26

(16) Zimmerman, P. M. Single-ended transition state finding with the growing string method. *Journal of Computational Chemistry* **2015**, *36*, 601–611.

(17) Johnson, M. S.; Nimlos, M. R.; Ninnemann, E.; Laich, A.; Fioroni, G. M.; Kang, D.; Bu, L.; Ranasinghe, D.; Khanniche, S.; Goldsborough, S. S.; Vasu, S. S.; Green, W. H. Oxidation and pyrolysis of methyl propyl ether. *International Journal of Chemical Kinetics* **2021**, *53*, 915–938.

(18) Vijver, R. V. D.; Vandewiele, N. M.; Bhoorasingh, P. L.; Slakman, B. L.; Khanshan, F. S.; Carstensen, H. H.; Reyniers, M. F.; Marin, G. B.; West, R. H.; Geem, K. M. V. Automatic Mechanism and Kinetic Model Generation for Gas- and Solution-Phase Processes: A Perspective on Best Practices, Recent Advances, and Future Challenges. *International Journal of Chemical Kinetics* **2015**, *47*, 199–231.

(19) Gao, C. W.; Allen, J. W.; Green, W. H.; West, R. H. Reaction Mechanism Generator: Automatic construction of chemical kinetic mechanisms. *Computer Physics Communications* **2016**, *203*, 212–225.

(20) Liu, M.; Grinberg Dana, A.; Johnson, M. S.; Goldman, M. J.; Jocher, A.; Payne, A. M.; Grambow, C. A.; Han, K.; Yee, N. W.; Mazeau, E. J.; Blondal, K.; West, R. H.; Goldsmith, C. F.; Green, W. H. Reaction Mechanism Generator v3.0: Advances in Automatic Mechanism Generation. *Journal of Chemical Information and Modeling* **2021**, *61*, 2686–2696.

(21) Johnson, M. et al. RMG Database for Chemical Property Prediction. *Journal of Chemical Information and Modeling 62*, 4906 – 4915.

(22) Johnson, M. S.; Pang, H.-W.; Liu, M.; Green, W. H. Species Selection for Automatic Chemical Kinetic Mechanism Generation. **2023**,

(23) Class, C. A.; Liu, M.; Vandeputte, A. G.; Green, W. H. Automatic mechanism gener-

ation for pyrolysis of di-tert-butyl sulfide. *Physical Chemistry Chemical Physics* **2016**, *18*, 21651–21658.

(24) Chu, T. C.; Buras, Z. J.; Oßwald, P.; Liu, M.; Goldman, M. J.; Green, W. H. Modeling of aromatics formation in fuel-rich methane oxy-combustion with an automatically generated pressure-dependent mechanism. *Physical Chemistry Chemical Physics* **2019**, *21*, 813–832.

(25) Zhang, P.; Yee, N. W.; Filip, S. V.; Hetrick, C. E.; Yang, B.; Green, W. H. Modeling study of the anti-knock tendency of substituted phenols as additives: An application of the reaction mechanism generator (RMG). *Physical Chemistry Chemical Physics* **2018**, *20*, 10637–10649.

(26) Dong, X.; Ninnemann, E.; Ranasinghe, D. S.; Laich, A.; Greene, R.; Vasu, S. S.; Green, W. H. Revealing the critical role of radical-involved pathways in high temperature cyclopentanone pyrolysis. *Combustion and Flame* **2020**, *216*, 280–292.

(27) Class, C. A.; Vasiliou, A. K.; Kida, Y.; Timko, M. T.; Green, W. H. Detailed kinetic model for hexyl sulfide pyrolysis and its desulfurization by supercritical water. *Physical Chemistry Chemical Physics* **2019**, *21*, 10311–10324.

(28) Dana, A. G.; Buesser, B.; Merchant, S. S.; Green, W. H. Automated Reaction Mechanism Generation Including Nitrogen as a Heteroatom. *International Journal of Chemical Kinetics* **2018**, *50*.

(29) Gillis, R. J.; Green, W. H. Thermochemistry Prediction and Automatic Reaction Mechanism Generation for Oxygenated Sulfur Systems: A Case Study of Dimethyl Sulfide Oxidation. *ChemSystemsChem* **2020**, *2*, e1900051.

(30) Farina, D. S.; Sirumalla, S. K.; Mazeau, E. J.; West, R. H. Extensive High-Accuracy Thermochemistry and Group Additivity Values for Halocarbon Combustion Modeling. *Industrial and Engineering Chemistry Research* **2021**, *60*, 15492–15501.

(31) Jalan, A.; Ashcraft, R. W.; West, R. H.; Green, W. H. Predicting solvation energies for kinetic modeling. Annual Reports on the Progress of Chemistry - Section C. 2010; pp 211–258.

(32) Jalan, A.; West, R. H.; Green, W. H. An extensible framework for capturing solvent effects in computer generated kinetic models. *Journal of Physical Chemistry B* **2013**, *117*, 2955–2970.

(33) Chung, Y.; Gillis, R. J.; Green, W. H. Temperature-dependent vapor–liquid equilibria and solvation free energy estimation from minimal data. *AIChE Journal* **2020**, *66*, e16976.

(34) Chung, Y.; Vermeire, F. H.; Wu, H.; Walker, P. J.; Abraham, M. H.; Green, W. H. Group Contribution and Machine Learning Approaches to Predict Abraham Solute Parameters, Solvation Free Energy, and Solvation Enthalpy. 2022.

(35) Goldsmith, C. F.; West, R. H. Automatic Generation of Microkinetic Mechanisms for Heterogeneous Catalysis. *Journal of Physical Chemistry C* **2017**, *121*, 9970–9981.

(36) Blondal, K.; Jelic, J.; Mazeau, E.; Studt, F.; West, R. H.; Goldsmith, C. F. Computer-Generated Kinetics for Coupled Heterogeneous/Homogeneous Systems: A Case Study in Catalytic Combustion of Methane on Platinum. *Industrial and Engineering Chemistry Research* **2019**, *58*, 17682–17691.

(37) Kreitz, B.; Sargsyan, K.; Blöndal, K.; Mazeau, E. J.; West, R. H.; Wehinger, G. D.; Turek, T.; Goldsmith, C. F. Quantifying the Impact of Parametric Uncertainty on Automatic Mechanism Generation for CO 2 Hydrogenation on Ni(111) . *JACS Au* **2021**, *1*, 1656–1673.

(38) Mazeau, E. J.; Satpute, P.; Blöndal, K.; Goldsmith, C. F.; West, R. H. Automated Mechanism Generation Using Linear Scaling Relationships and Sensitivity Analyses

Applied to Catalytic Partial Oxidation of Methane. *ACS Catalysis* **2021**, *11*, 7114–7125.

(39) Grinberg Dana, A.; Liu, M.; Green, W. H. Automated chemical resonance generation and structure filtration for kinetic modeling. *International Journal of Chemical Kinetics* **2019**, *51*, 760–776.

(40) Grambow, C. A.; Li, Y. P.; Green, W. H. Accurate Thermochemistry with Small Data Sets: A Bond Additivity Correction and Transfer Learning Approach. *Journal of Physical Chemistry A* **2019**, *123*, 5826–5835.

(41) Grinberg Dana, A.; Ranasinghe, D.; Wu, O. H.; Grambow, C.; Dong, X.; Johnson, M. S.; Goldman, M.; Liu, M.; Green, W. H. ARC - Automated Rate Calculator. `https://github.com/ReactionMechanismGenerator/ARC`.

(42) Landrum, G. RDKit. **2010**,

(43) Dana, A. G. et al. Automated reaction kinetics and network exploration (Arkane): A statistical mechanics, thermodynamics, transition state theory, and master equation software. *International Journal of Chemical Kinetics* **2023**, *55*, 300–323.

(44) Alvarez-Idaboy, J. R.; Mora-Diez, N.; Vivier-Bunge, A. A quantum chemical and classical transition state theory explanation of negative activation energies in OH addition to substituted ethenes. *Journal of the American Chemical Society* **2000**, *122*, 3715–3720.

(45) Greenwald, E. E.; North, S. W.; Georgievskii, Y.; Klippenstein, S. J. A two transition state model for radical-molecule reactions: A case study of the addition of OH to C 2H 4. *Journal of Physical Chemistry A* **2005**, *109*, 6031–6044.

(46) Abraham, M. H.; Ibrahim, A.; Zissimos, A. M. Determination of sets of solute descriptors from chromatographic measurements. 2004.

(47) Abraham, M. H.; Acree, W. E. Correlation and prediction of partition coefficients between the gas phase and water, and the solvents dodecane and undecane. *New Journal of Chemistry* **2004**, *28*, 1538–1543.

(48) Abraham, M. H.; Acree, W. E. Estimation of heat capacities of gases, liquids and solids, and heat capacities of vaporization and of sublimation of organic chemicals at 298.15 K. *Journal of Molecular Liquids* **2020**, *317*, 113969.

(49) Abraham, M. H.; Acree, W. E. Estimation of enthalpies of sublimation of organic, organometallic and inorganic compounds. *Fluid Phase Equilibria* **2020**, *515*, 112575.

(50) Cramer, C. J.; Truhlar, D. G. Molecular Orbital Theory Calculations of Aqueous Solvation Effects on Chemical Equilibria. *Journal of the American Chemical Society* **1991**, *113*, 8552–8554.

(51) Marenich, A. V.; Olson, R. M.; Kelly, C. P.; Cramer, C. J.; Truhlar, D. G. Self-consistent reaction field model for aqueous and nonaqueous solutions based on accurate polarized partial charges. *Journal of Chemical Theory and Computation* **2007**, *3*, 2011–2033.

(52) Marenich, A. V.; Cramer, C. J.; Truhlar, D. G. Universal solvation model based on solute electron density and on a continuum model of the solvent defined by the bulk dielectric constant and atomic surface tensions. *Journal of Physical Chemistry B* **2009**, *113*, 6378–6396.

(53) Klamt, A. Conductor-like screening model for real solvents: A new approach to the quantitative calculation of solvation phenomena. *Journal of Physical Chemistry* **1995**, *99*, 2224–2235.

(54) Klamt, A.; Jonas, V.; Bürger, T.; Lohrenz, J. C. Refinement and parametrization of COSMO-RS. *Journal of Physical Chemistry A* **1998**, *102*, 5074–5085.

31

(55) Klamt, A.; Eckert, F. COSMO-RS: a novel and efficient method for the a priori prediction of thermophysical data of liquids. *Fluid Phase Equilibria* **2000**, *172*, 43–72.

(56) Johnson, M. S.; Gierada, M.; Hermes, E. D.; Bross, D. H.; Sargsyan, K.; Najm, H. N.; Zádor, J. Pynta—An Automated Workflow for Calculation of Surface and Gas-Surface Kinetics. *Journal of Chemical Information and Modeling* **2023**, *63*, 5153–5168.

(57) Wellendorff, J.; Lundgaard, K. T.; Møgelhøj, A.; Petzold, V.; Landis, D. D.; Nørskov, J. K.; Bligaard, T.; Jacobsen, K. W. Density functionals for surface science: Exchange-correlation model development with Bayesian error estimation. *Physical Review B* **2012**, *85*, 235149.

(58) Farina, D. S.; Sirumalla, S. K.; West, R. H. Automating the generation of detailed kinetic models for halocarbon combustion with the Reaction Mechanism Generator. *Proceedings of the Combustion Institute* **2023**, *39*, 223–232.

(59) Ruscic, B.; Pinzon, R. E.; Laszewski, G. V.; Kodeboyina, D.; Burcat, A.; Leahy, D.; Montoy, D.; Wagner, A. F. Active Thermochemical Tables: thermochemistry for the 21st century. *Journal of Physics: Conference Series* **2005**, *16*, 561.

(60) ATcT Thermochemical Values ver. 1.124. `https://atct.anl.gov/Thermochemical%20Data/version%201.124/index.php`.

(61) Johnson, M. S.; Green, W. H. A Machine Learning Based Approach to Reaction Rate Estimation. *ChemRxiv* **2022**,

(62) Zhang, Y.; Viswanathan, V. Not all fluorination is the same: Unique effects of fluorine functionalization of ethylene carbonate for tuning solid-electrolyte interphase in li metal batteries. *Langmuir* **2020**, *36*, 11450–11466.

(63) Hansen, H. A.; Viswanathan, V.; NØrskov, J. K. Unifying kinetic and thermodynamic

analysis of 2 e- and 4 e - reduction of oxygen on metal surfaces. *Journal of Physical Chemistry C* **2014**, *118*, 6706–6718.

(64) López-Estrada, O.; Laguna, H. G.; Barrueta-Flores, C.; Amador-Bedolla, C. Reassessment of the Four-Point Approach to the Electron-Transfer Marcus-Hush Theory. *ACS Omega* **2018**, *3*, 2130–2140.

(65) Leffler, J. E. Parameters for the description of transition states. 1953; `https://www.science.org/doi/10.1126/science.117.3039.340`.

(66) Johnson, M. S.; Pang, H.-W.; Payne, A. M.; Green, W. H. ReactionMechanismSimulator.jl: A Modern Approach to Chemical Kinetic Mechanism Simulation and Analysis. **2023**,

(67) Johnson, M. S.; McGill, C. J.; Green, W. H. Transitory Sensitivity in Automatic Chemical Kinetic Mechanism Analysis. **2022**,

(68) Yamada, Y.; Furukawa, K.; Sodeyama, K.; Kikuchi, K.; Yaegashi, M.; Tateyama, Y.; Yamada, A. Unusual stability of acetonitrile-based superconcentrated electrolytes for fast-charging lithium-ion batteries. *Journal of the American Chemical Society* **2014**, *136*, 5039–5046.

(69) Dhattarwal, H. S.; Chen, Y. W.; Kuo, J. L.; Kashyap, H. K. Mechanistic insight on the formation of a solid electrolyte interphase (SEI) by an acetonitrile-based superconcentrated [Li][TFSI] electrolyte near lithium metal. *Journal of Physical Chemistry C* **2020**, *124*, 27495–27502.

(70) Takenaka, N.; Fujie, T.; Bouibes, A.; Yamada, Y.; Yamada, A.; Nagaoka, M. Microscopic Formation Mechanism of Solid Electrolyte Interphase Film in Lithium-Ion Batteries with Highly Concentrated Electrolyte. *Journal of Physical Chemistry C* **2018**, *122*, 2564–2571.

(71) Zhuang, G. V.; Xu, K.; Yang, H.; Jow, T. R.; Ross, P. N. Lithium ethylene dicarbonate identified as the primary product of chemical and electrochemical reduction of EC in 1.2 M LiPF 6/EC:EMC electrolyte. *Journal of Physical Chemistry B* **2005**, *109*, 17567–17573.

(72) Pang, H. W.; Dong, X.; Johnson, M. S.; Green, W. H. Subgraph Isomorphic Decision Tree to Predict Radical Thermochemistry with Bounded Uncertainty Estimation. *Journal of Physical Chemistry A* **2024**, *128*, 2891–2907.

(73) Johnson, M. S.; Mueller, J. N.; Daniels, C.; Najm, H. N.; Zádor, J. Diffusion Limited Kinetics Accounting for Reactive Species in 3D, 2D, and at 2D/3D Interfaces. **2023**,